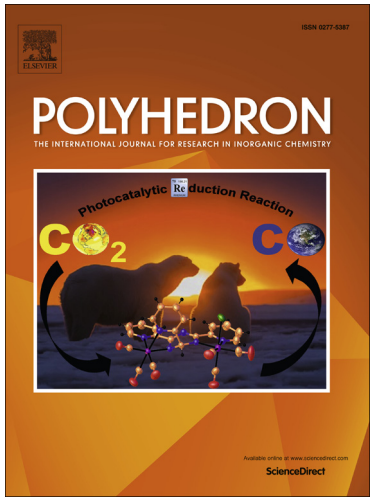

Synthesis, structural, DFT calculations and biological studies of rhodium and iridium complexes containing azine Schiff-base ligands

Sanjay Adhikari, Dipankar Sutradhar, Samantha L. Shepherd, Roger M. Phillips, Asit K. Chandra, K. Mohan Rao

PII: S0277-5387(16)30218-2
DOI: http://dx.doi.org/10.1016/j.poly.2016.06.001
Reference: POLY 12039

To appear in: *Polyhedron*

Received Date: 4 May 2016
Accepted Date: 1 June 2016

Please cite this article as: S. Adhikari, D. Sutradhar, S.L. Shepherd, R.M. Phillips, A.K. Chandra, K. Mohan Rao, Synthesis, structural, DFT calculations and biological studies of rhodium and iridium complexes containing azine Schiff-base ligands, *Polyhedron* (2016), doi: http://dx.doi.org/10.1016/j.poly.2016.06.001

Synthesis, structural, DFT calculations and biological studies of rhodium and iridium complexes containing azine Schiff-base ligands

Sanjay Adhikari[a], Dipankar Sutradhar[a], Samantha L. Shepherd[b], Roger M Phillips[b], Asit K. Chandra[a], K. Mohan Rao[a*]

[a]Centre for Advanced Studies in Chemistry, North-Eastern Hill University, Shillong 793 022, India.

E-mail: mohanrao59@gmail.com

Telephone Number: +91 364 2722620

Fax Number: +91 364 2550076

[b]Department of Pharmacy, School of Applied Sciences, University of Huddersfield, Huddersfield HD1 3DH, UK

Graphical abstract

Half-sandwich Cp*Rh(III) and Cp*Ir(III) complexes have been synthesized with N-N′ azine Schiff-base ligands and characterized by spectroscopic techniques. The molecular structures of some of the representative complexes have been confirmed by single crystal X-ray analysis. Chemo-sensitivity activities of the complexes were evaluated against HT-29 (human colorectal cancer) cell line and non-cancer cell line ARPE-19 (human retinal epithelial cells).

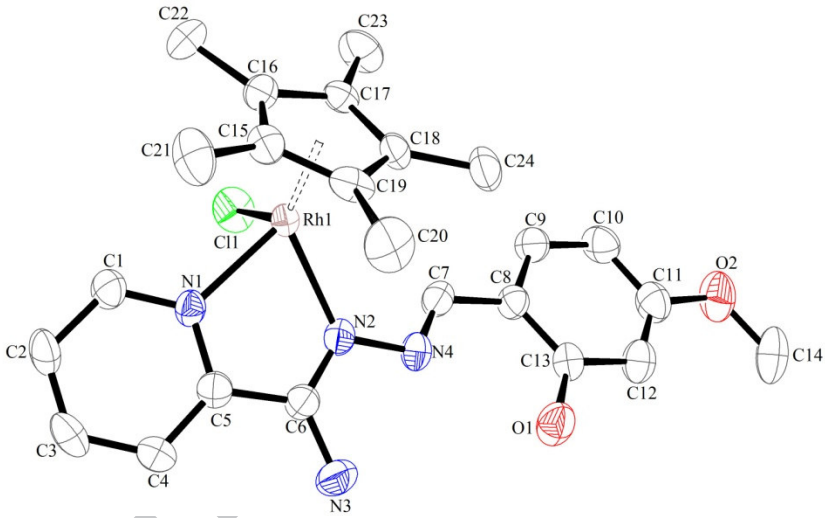

Complex **1**

Abstract

The reaction of $[Cp^*MCl_2]_2$ (M = Rh/Ir) with N-N′ azine Schiff-base ligands (L1-L4) leads to the formation of mononuclear cationic half-sandwich complexes having the general formula $[Cp^*M(L)Cl]^+$ (**1**–**8**), (M = Rh/Ir and L = (2-hydroxy-4-methoxybenzylidene)2-pyridylamidrazone (L1), (2-hydroxybenzylidene)2-pyridylamidrazone (L2), (1-(2-hydroxyphenyl)ethylidene)2-pyridylamidrazone (L3) and (1-phenylethylidene)2-pyridylamidrazone (L4). All these complexes were isolated as their hexafluorophosphate salts and fully characterized by spectroscopic and analytical techniques. The molecular structure of complexes (**1**), (**3**), (**4**), (**7**) and (**8**) have been determined by single crystal X-ray crystallographic studies which displayed the coordination of the ligand to the metal in a bidentate N∩N fashion through nitrogen atom of pyridine and one azine nitrogen. The chemo-sensitivity activities of the complexes were evaluated against HT-29 (human colorectal cancer) cell line and non-cancer cell line ARPE-19 (human retinal epithelial cells) which revealed that the complexes are moderately cytotoxic to cancer cells over human cells although complex **5** was the most potent among all the compounds. Theoretical studies carried out using DFT and TD-DFT at B3LYP level shows good agreement with the experimental results.

Keywords: Rhodium, Iridium, Azine Schiff-base ligands, Cytotoxicity

1. Introduction

The chemistry of half-sandwich organometallic complexes has evolved as a versatile subject of research during the past few decades due to its wide application in biological and medicinal fields [1-4]. Organometallic half-sandwich compounds of the general formula [Cp*MCl(LL´)] (M = Rh, Ir and LL' = N,N or N,O donor ligands) have been extensively studied for their cytostatic activity, DNA binding, cellular uptake and as DNA intercelators [5-9]. Rhodium and iridium complexes have also been investigated as an alternative to platinum based drugs mainly because of their water solubility and lability towards ligand exchange [10, 11]. Recently Therrien *et.al* reported dinuclear dithiolato bridged rhodium and iridium complexes which exhibit cytotoxicity against human ovarian cancer cells lines (A2780 and A2780cisR) [12]. C-H activated cyclometallated Rh(III) and Ir(III) complexes can effectively bind to DNA and protein through electrostatic and hydrophobic interactions [13]. Iridium complexes of dihydroxybipyridine are active catalysts for homogenous water oxidation under mild reaction conditions [14]. Rh(III) and Ir(III) polypyridyl complexes exhibits strong antiproliferative activity towards human cancer cell lines and are also capable of binding to DNA [15]. A number of half-sandwich Ir(III) complexes have been reported by Sadler *et al* with chelating C, N and pyridine ligands and N, N donor ligands which showed strong antiproliferative activity [16, 17].

Pyridyl azines represent an important class of organic compounds with interesting properties having wide applications in various areas [18]. Open chain diazine Schiff base ligands linked by a single N-N bond are of great interest due to its rotational flexibility around the N-N bond and potential donor sites which can give rise to a rich variety of coordination compounds with different binding modes [19]. The N-N bridging ligand plays a crucial role in communicating the metal centers to form mononuclear, dinuclear or polynuclear complexes [20].

The diazine ligand has been employed into several transition metal azido and thiocyanato systems namely Mn(II)-azido, Cd(II)-NCS to obtain several 1D, 2D and 3D polymers which exhibit interesting magnetic properties [21, 22]. Dinuclear transition metal complexes of Cu, Zn, Mn and Ni have been reported with bridging N-N diazine ligands which give rise to strong ferromagnetic and antiferromagnetic coupling [23]. In the recent years our group has reported many half-sandwich Ru(II), Rh(III) and Ir(III) complexes with azine ligands [24, 25]. In continuation with our interest of these ligands herein we report four new azine Schiff base ligands derived from 2-pyridylamidrazone and its corresponding rhodium and iridium half-sandwich metal complexes. The complexes were tested for their cytotoxic property to selectively kill HT-29 cancer cell line against normal ARPE-19 cells.

2. Experimental Section

2. 1. Physical methods and materials

All the reagents were purchased from commercial sources and used as received. Starting materials $RhCl_3.nH_2O$, $IrCl_3.nH_2O$ were purchased from Arora Matthey limited. 2-cyanopyridine, 2-hydroxybenzaldehyde, 2-hydroxyacetophenone, were obtained from Aldrich, acetophenone and 2-hydroxy-4-methoxybenzaldehyde were obtained from Alfa-Aesar. The solvents were purified and dried according to standard procedures [26]. All the reactions were carried out under normal conditions. The starting precursor metal complexes $[Cp^*MCl_2]_2$ (M = Rh/Ir) were prepared according to the literature methods [27]. Infrared spectra were recorded on a Perkin-Elmer 983 spectrophotometer by using KBr pellets in the range of 400-4000 cm^{-1}. ^1H NMR spectra were recorded on a Bruker Avance II 400 MHz spectrometer using DMSO-d_6 and $CDCl_3$ as solvents. Absorption spectra were recorded on a Perkin-Elmer Lambda 25 UV/Visible spectrophotometer in the range of 200-800 nm at room temperature in acetonitrile. Elemental

analyses of the complexes were performed on a Perkin-Elmer 2400 CHN/S analyzer. Mass spectra were recorded using Q-Tof APCI-MS instrument (model HAB 273). All these mononuclear metal complexes were synthesized and characterized by using FT-IR, ^{1}H NMR, UV-Vis, and Single-crystal X-ray diffraction techniques.

2. 2. Single-crystal X-ray structures analyses

The orange crystals of complexes (**1**), (**3**), (**7**) and (**8**) were obtained by slow diffusion of hexane into acetone or DCM solution and yellow crystals of complex (**4**) was obtained by diffusing hexane into DCM solution. Single crystal X-ray diffraction data for all the complexes (**1**), (**3**) (**4**), (**7**) and (**8**) were collected on a Oxford Diffraction Xcalibur Eos Gemini diffractometer at 293 K using graphite monochromated Mo-Kα radiation (λ = 0.71073 Å). The strategy for the data collection was evaluated using the CrysAlisPro CCD software. Crystal data were collected by standard ''phi–omega scan'' techniques and were scaled and reduced using CrysAlisPro RED software. The structures were solved by direct methods using SHELXS-97 and refined by full-matrix least squares with SHELXL-97 refining on F^2 [28, 29]. The positions of all the atoms were obtained by direct methods. Metal atoms in the complex were located from the E-maps and non-hydrogen atoms were refined anisotropically. The hydrogen atoms bound to the carbon were placed in geometrically constrained positions and refined with isotropic temperature factors, generally 1.2 U_{eq} of their parent atoms. Crystallographic and structure refinement details for the complexes are summarized in Table 1, and selected bond lengths and bond angles are presented in Table S1. Figures 1-3 were drawn with ORTEP3 program. Figure 4 and Figures S3-S6 were drawn with MERCURY3.6 program [30].

2.3. Biological studies

All complexes (**1**-**8**) were dissolved in DMSO at 100 mM and stored at -20 °C until needed. The complexes were tested against cancer cell line HT-29 (human colorectal cancer), and one non-cancer cell line ARPE-19 (human retinal epithelial cells). Cells were seeded into 96 well plates at 1 x 10^3 cells per well and incubated at 37 °C in a CO_2 enriched (5%), humidified atmosphere overnight to adhere. The cells were exposed to a range of drug concentrations in the range of 0-100 µM for four days before cell survival was determined using the MTT assay [31]. To each well MTT (0.5 mg/ml) was added and was further incubated at 37 °C for 4 h. After this the MTT was removed from each well and the formazan crystals formed were dissolved in 150 µM DMSO. The absorbance of the resulting solution was recorded at 550 nm using an ELISA spectrophotometer. The percentage of cell inhibition was calculated by dividing the absorbance of treated cell by the control value absorbance (exposed to 0.1 % DMSO). The results were expressed in terms of IC_{50} values (concentration required to kill 50 % cell) and all studies were performed in triplicate. The results were also expressed in terms of a 'selectivity index' defined as the IC_{50} of the non-cancer cell line ARPE divided by the IC_{50} of cancer cell lines [32]. Values greater than 1 demonstrate that the compound is preferentially active against tumor cell compared to normal cell lines.

2.4. Computational methodology

All the electronic structure calculations of the metal complexes (**1**-**8**) were carried out using the Gaussian 09 suite of program [33]. The geometries of the rhodium and iridium complexes were optimized in the gas phase employing the DFT-based B3LYP method with 6-31G** basis set for (H, C, N, O, Cl, F and P atoms and LANL2DZ [34, 35] for (Rh and Ir) atoms. Harmonic frequency calculations were carried out at the same level of theory to ensure that the optimized geometries were true minima on the potential energy surface (PES). Natural

Bond Orbital (NBO) analysis [36] was used to obtain the charge distribution on individual atoms and the d-orbital occupations of the metal present in the complexes. Time dependent-Density Functional Theory (TD-DFT) [37] has been employed to evaluate the absorption spectra and the electronic transitions of the metal complexes. In order to incorporate the effect of the solvent around the molecule, the Polarizable Continuum Model (PCM) [38] was used in TD-DFT calculations. The percentage contribution of molecular orbital analysis was carried out using Chemissian software package [39].

2.4. General procedure for preparation of ligands 1-4

2.4.1. The azine Schiff base ligands (L1-L4) were prepared by two step procedure.

In the first step 2-pyridylamidrazone was prepared, by following a reported procedure [40]. 2-cyanopyridine and hydrazine hydrate were dissolved and stirred in absolute ethanol overnight to give 2-pyridylamidrazone as yellow crystalline solid which was used in the next step without further purification (Scheme-1). In the second step (5 mmol) of aldehyde or ketone and 2-pyridylamidrazone (5 mmol) was refluxed in 10 ml ethanol for 5 hours (Scheme-2). The products obtained after cooling the solution were filtered off washed with cold methanol and diethyl ether and dried in vacuum.

Data for ligands (L1-L4)

2.4.2. (2-hydroxy-4-methoxybenzylidene)2-pyridylamidrazone (L1)

Color: Yellow needles; Yield: 88%; IR (KBr, cm^{-1}): 3487(s), 3380(s), 3333(m), 2964(m), 1627(s), 1587(m), 1566(m), 1394(m), 1340(s); ^1H NMR (400 MHz, $CDCl_3$): δ = 11.82 (s, 1H, OH), 8.60 (s, 1H, $CH_{(imine)}$), 8.57 (d, 1H, J = 4.0 Hz, $CH_{(py)}$), 8.34 (d, 1H, J = 8.0 Hz, $CH_{(py)}$), 7.76 (t, 1H, $CH_{(py)}$), 7.35 (t, 1H, $CH_{(py)}$), 7.20 (d, 2H, J = 8.0 Hz, $CH_{(Ar)}$), 6.46-6.50 (m, 3H, NH_2, $CH_{(Ar)}$), 3.80 (s, 3H, OMe); HRMS-APCI (m/z): 271.11 $[M+H]^+$; UV–Vis {Acetonitrile, λ_{max},

nm (ε/10^{-4} M^{-1} cm^{-1})}: 218 (0.84), 314 (0.68), 342 (0.92), 355 (0.94); Anal. Calc. for $C_{14}H_{14}N_4O_2$ (270.29): C, 62.21; H, 5.22; N, 20.73. Found: C, 62.36; H, 5.35; N, 20.86%.

2.4.3. (2-hydroxybenzylidene)2-pyridylamidrazone (L2)

Color: Yellow needles; Yield: 92%; IR (KBr, cm^{-1}): 3477(s), 3363(s), 3340(s), 3043(m), 1626(s), 1576(m), 1567(m), 1473(m), 1337(m); ^{1}H NMR (400 MHz, $CDCl_3$): δ = 11.61 (s, 1H, OH), 8.59 (s, 1H, $CH_{(imine)}$), 8.54 (d, 1H, *J* = 4.0 Hz, $CH_{(py)}$), 8.28 (d, 1H, *J* = 8.0 Hz, $CH_{(py)}$), 7.74 (t, 1H, $CH_{(py)}$), 7.33 (t, 1H, $CH_{(py)}$), 7.24-7.27 (m, 3H, NH_2, $CH_{(Ar)}$), 6.96 (d, 1H, *J* = 8.0 Hz, $CH_{(Ar)}$), 6.87 (t, 2H, $CH_{(Ar)}$); HRMS-APCI (m/z): 241.10 $[M+H]^+$; UV–Vis {Acetonitrile, λ_{max}, nm (ε/10^{-4} M^{-1} cm^{-1})}: 219 (0.84), 247 (0.55), 349 (1.30), 361 (1.29); Anal. Calc. for $C_{13}H_{12}N_4O$ (240.26): C, 64.99; H, 5.03; N, 23.32. Found: C, 65.12; H, 5.18; N, 23.44%.

2.4.4. (1-(2-hydroxyphenyl)ethylidene)2-pyridylamidrazone (L3)

Color: Yellow crystalline solid; Yield: 95%; IR (KBr, cm^{-1}): 3482(s), 3339(s), 3056(m), 3003(m), 1615(s), 1562(m), 1507(m), 1300(m); ^{1}H NMR (400 MHz, $CDCl_3$): δ = 13.73 (s, 1H, OH), 8.59 (d, 1H, *J* = 4.0 Hz, $CH_{(py)}$), 8.36 (d, 1H, *J* = 8.0 Hz, $CH_{(py)}$), 7.79 (t, 1H, $CH_{(py)}$), 7.58 (t, 1H, $CH_{(py)}$), 7.21-7.28 (m, 3H, NH_2, $CH_{(Ar)}$), 6.98 (d, 2H, *J* = 8.0 Hz, $CH_{(Ar)}$), 6.89 (t, 1H, $CH_{(Ar)}$), 2.62 (s, 3H, CH_3); HRMS-APCI (m/z): 255.12 $[M+H]^+$; UV–Vis {Acetonitrile, λ_{max}, nm (ε/10^{-4} M^{-1} cm^{-1})}: 217 (1.21), 303 (0.74), 344 (0.95); Anal. Calc. for $C_{14}H_{14}N_4O$ (254.29): C, 66.13; H, 5.55; N, 22.03. Found: C, 66.25; H, 5.68; N, 22.21%.

2.4.5. (1-phenylethylidene)2-pyridylamidrazone (L4)

Color: Yellow crystalline solid; Yield: 92%; IR (KBr, cm^{-1}): 3450(s), 3331(s), 3056(m), 3009(m), 1604(s), 1568(m), 1445(m), 1362(m); ^{1}H NMR (400 MHz, $CDCl_3$): δ = 8.58 (d, 1H, *J* = 4.0 Hz, $CH_{(py)}$), 8.23 (d, 1H, *J* = 8.0 Hz, $CH_{(py)}$), 7.71 (t, 1H, $CH_{(py)}$), 7.30 (t, 1H, $CH_{(py)}$), 7.21-7.28 (m, 3H, NH_2, $CH_{(Ar)}$), 6.93 (m, 3H, $CH_{(Ar)}$), 6.89 (t, 1H, $CH_{(Ar)}$), 2.39 (s, 3H, CH_3); HRMS-

APCI (m/z): 239.13 $[M+H]^+$; UV–Vis {Acetonitrile, λ_{max}, nm ($\varepsilon/10^{-4}$ M^{-1} cm^{-1})}: 225 (0.21), 327 (0.29); Anal. Calc. for $C_{14}H_{14}N_4$ (238.29): C, 70.57; H, 5.92; N, 23.51. Found: C, 70.72; H, 6.03; N, 23.62%.

2.5. General procedure for preparation of metal complexes (1-8)

A mixture of metal precursor $[Cp^*MCl_2]_2$ (M = Rh/Ir) (0.1 mmol), azine Schiff-base ligands (L1-L4) (0.2 mmol) and 2.5 equivalents of NH_4PF_6 in dry methanol (10 ml) was stirred at room temperature for 8 hours (Scheme-3). The solvent was evaporated under reduced pressure, and the residue was dissolved in dichloromethane and filtered over celite to remove excess salt. The filtrate was reduced to 2 ml and diethyl ether was added to induce precipitation. The yellow colored precipitate, which formed, was filtered and washed with diethyl ether and dried in vacuum.

*2.5.1. [Cp*Rh(L1)Cl]PF_6 (**1**)*

Yield: 56 mg (40%); IR (KBr, cm^{-1}): 3460(m), 3237(m), 2926(w), 1630(s), 1595(m), 1296(m), 846(s); ^{1}H NMR (400 MHz, $CDCl_3$): δ = 10.5 (s, 1H, OH), 9.02 (s, 1H, $CH_{(imine)}$), 8.76 (d, 1H, *J* = 4.0 Hz, $CH_{(py)}$), 8.54 (d, 1H, *J* = 4.0 Hz, $CH_{(py)}$), 8.13 (t, 1H, $CH_{(py)}$), 7.76 (t, 1H, $CH_{(py)}$), 7.41 (d, 1H, *J* = 8.0 Hz, $CH_{(Ar)}$), 7.38 (s, 2H, NH_2), 6.53 (d, 1H, *J* = 8.0 Hz, $CH_{(Ar),}$), 6.50 (s, 1H, $CH_{(Ar)}$), 3.81 (s, 3H, OMe), 1.58 (s, 15H, $CH_{(Cp^*)}$); HRMS-APCI (m/z): 507.12 $[M\text{-}PF_6\text{-}HCl]^+$; UV–Vis {Acetonitrile, λ_{max}, nm ($\varepsilon/10^{-4}$ M^{-1} cm^{-1})}: 233 (0.98), 277 (0.57), 352 (0.42); Anal. Calc. for $C_{24}H_{29}ClF_6N_4O_2PRh$ (688.84): C, 41.85; H, 4.24; N, 8.13. Found: C, 41.96; H, 4.16; N, 8.23%.

*2.5.2. [Cp*Ir(L1)Cl]PF_6 (**2**)*

Yield: 70 mg (45%); IR (KBr, cm^{-1}): 3447(m), 3241(m), 2925(m), 1630(s), 1610(m), 1293(m), 846(s); ^{1}H NMR (400 MHz, $CDCl_3$): δ = 10.4 (s, 1H, OH), 9.02 (s, 1H, $CH_{(imine)}$), 8.77 (d, 1H, *J*

= 4.0 Hz, $CH_{(py)}$), 8.51 (d, 1H, *J* = 4.0 Hz, $CH_{(py)}$), 8.17 (t, 1H, $CH_{(py)}$), 7.78 (t, 1H, $CH_{(py)}$), 7.42 (d, 1H, *J* = 8.0 Hz, $CH_{(Ar)}$), 7.39 (s, 2H, NH_2), 6.56 (d, 1H, *J* = 8.0 Hz, $CH_{(Ar)}$), 6.54 (s, 1H, $CH_{(Ar)}$), 3.87 (s, 3H, OMe), 1.62 (s, 15H, $CH_{(Cp^*)}$); HRMS-APCI (m/z): 597.18 $[M\text{-}PF_6\text{-}HCl]^+$; UV–Vis {Acetonitrile, λ_{max}, nm ($\varepsilon/10^{-4}$ M^{-1} cm^{-1})}: 266 (0.36), 347 (0.29); Anal. Calc. for $C_{24}H_{29}ClF_6N_4O_2PIr$ (778.14): C, 37.04; H, 3.76; N, 7.20. Found: C, 37.19; H, 3.89; N, 7.31%.

*2.5.3. [Cp*Rh(L2)Cl]PF_6 (**3**)*

Yield: 52 mg (39%); IR (KBr, cm^{-1}): 3422(m), 3310(w), 2923(w), 1636(s), 1603(m), 1457(m), 845(s); ^{1}H NMR (400 MHz, $CDCl_3$): δ = 10.1 (s, 1H, OH), 9.11 (s, 1H, $CH_{(imine)}$), 8.78 (d, 1H, *J* = 4.0 Hz, $CH_{(py)}$), 8.49 (d, 1H, *J* = 8.0 Hz, $CH_{(py)}$), 8.14 (t, 2H, $CH_{(py)}$), 7.78 (t, 1H, $CH_{(Ar)}$), 7.60 (d, 1H, *J* = 8.0 Hz, $CH_{(Ar)}$), 7.38 (s, 2H, NH_2), 6.92-7.01 (m, 2H, $CH_{(Ar)}$), 1.58 (s, 15H, $CH_{(Cp^*)}$); HRMS-APCI (m/z): 477.12 $[M\text{-}PF_6\text{-}HCl]^+$; UV–Vis {Acetonitrile, λ_{max}, nm ($\varepsilon/10^{-4}$ M^{-1} cm^{-1})}: 235 (1.55), 283 (0.79), 348 (1.00); Anal. Calc. for $C_{23}H_{27}ClF_6N_4OPRh$ (658.81): C, 41.93; H, 4.13; N, 8.50. Found: C, 42.08; H, 4.25; N, 8.68%.

*2.5.4. [Cp*Ir(L2)Cl]PF_6 (**4**)*

Yield: 52 mg (34%); IR (KBr, cm^{-1}): 3479(s), 3329(s), 2924(w), 1642(s), 1618(m), 1602(m), 842(s); ^{1}H NMR (400 MHz, $CDCl_3$): δ = 10.1 (s, 1H, OH), 9.13 (s, 1H, $CH_{(imine)}$), 8.80 (d, 1H, *J* = 4.0 Hz, $CH_{(py)}$), 8.56 (d, 1H, *J* = 8.0 Hz, $CH_{(py)}$), 8.18 (t, 2H, $CH_{(py)}$), 7.80 (t, 1H, $CH_{(Ar)}$), 7.64 (d, 1H, *J* = 8.0 Hz, $CH_{(Ar)}$), 7.40 (s, 2H, NH_2), 6.99-7.35 (m, 2H, $CH_{(Ar)}$), 1.63 (s, 15H, $CH_{(Cp^*)}$); HRMS-APCI (m/z): 567.17 $[M\text{-}PF_6\text{-}HCl]^+$; UV–Vis {Acetonitrile, λ_{max}, nm ($\varepsilon/10^{-4}$ M^{-1} cm^{-1})}: 291 (0.62), 344 (0.78); Anal. Calc. for $C_{23}H_{27}ClF_6N_4OPIr$ (748.12): C, 36.93; H, 3.64; N, 7.49. Found: C, 37.11; H, 3.83; N, 7.62%.

*2.5.5. [(Cp*Rh(L3)Cl]PF_6 (**5**)*

Yield: 58 mg (43%); IR (KBr, cm^{-1}): 3452(s), 3318(s), 2924(m), 1648(s), 1600(m), 1566(m), 1489(m), 842(s); ^1H NMR (400 MHz, DMSO-d_6): δ = 12.5 (s, 1H, OH), 8.96 (d, 1H, *J* = 4.0 Hz, $CH_{(py)}$), 8.33-8.38 (m, 3H, $CH_{(py)}$), 7.91 (t, 1H, $CH_{(Ar)}$), 7.86 (d, 1H, *J* = 8.0 Hz, $CH_{(Ar)}$), 7.48 (t, 1H, J = 8.0 Hz, $CH_{(Ar)}$), 7.01-7.06 (m, 3H, NH_2, $CH_{(Ar)}$), 2.48 (s, 3H, CH_3), 1.59 (s, 15H, $CH_{(Cp^*)}$); HRMS-APCI (m/z): 491.14 $[M\text{-}PF_6\text{-}HCl]^+$; UV–Vis {Acetonitrile, λ_{max}, nm ($\varepsilon/10^{-4}$ M^{-1} cm^{-1})}: 229 (0.95), 268 (0.59), 332 (0.32); Anal. Calc. for $C_{24}H_{29}ClF_6N_4OPRh$ (672.84): C, 42.84; H, 4.34; N, 8.33. Found: C, 42.98; H, 4.26; N, 8.48%.

*2.5.6. [Cp*Ir(L3)Cl]PF_6 (**6**)*

Yield: 65 mg (42%); IR (KBr, cm^{-1}): 3460(m), 3237(m), 2926(w), 1630(s), 1595(m), 1296(m), 846(s), 3456(m), 3369(m), 2925(m), 1649(s), 1618(m), 1598(m), 1306(m), 845(s); ^1H NMR (400 MHz, DMSO-d_6): δ = 12.3 (s, 1H, OH), 8.94 (d, 1H, *J* = 4.0 Hz, $CH_{(py)}$), 8.44 (d, 1H, *J* = 4.0 Hz, $CH_{(py)}$), 8.35 (t, 2H, $CH_{(py)}$), 7.90 (t, 1H, $CH_{(Ar)}$), 7.86 (d, 1H, *J* = 8.0 Hz, $CH_{(Ar)}$), 7.48 (t, 1H, $CH_{(Ar)}$), 7.01-7.06 (m, 3H, NH_2, $CH_{(Ar)}$), 2.46 (s, 3H, CH_3), 1.58 (s, 15H, $CH_{(Cp^*)}$); HRMS-APCI (m/z): 581.19 $[M\text{-}PF_6\text{-}HCl]^+$; UV–Vis {Acetonitrile, λ_{max}, nm ($\varepsilon/10^{-4}$ M^{-1} cm^{-1})}: 209 (1.27), 263 (0.66), 330 (0.36); Anal. Calc. for $C_{24}H_{29}ClF_6N_4OPIr$ (762.15): C, 37.82; H, 3.84; N, 7.35. Found: C, 37.96; H, 3.96; N, 7.44%.

*2.5.7. [(Cp*Rh(L4)Cl]PF_6 (**7**)*

Yield: 54 mg (41%); IR (KBr, cm^{-1}): 3441(s), 3137(m), 2961(w), 1640 (s), 1593(m), 1464(m), 841(s); ^1H NMR (400 MHz, DMSO-d_6): δ = 8.96 (d, 1H, *J* = 4.0 Hz, $CH_{(py)}$), 8.33-8.37 (m, 2H, $CH_{(py)}$), 7.88 (t, 1H, $CH_{(py)}$), 7.81 (d, 1H, *J* = 8.0 Hz, $CH_{(Ar)}$), 7.46 (t, 1H, $CH_{(Ar)}$), 7.23-7.28 (m, 2H, $CH_{(Ar)}$), 6.97-7.02 (m, 3H, NH_2, $CH_{(Ar)}$), 2.47 (s, 3H, CH_3), 1.59 (s, 15H, $CH_{(Cp^*)}$); HRMS-APCI (m/z): 511.12 $[M\text{-}PF_6]^+$; UV–Vis {Acetonitrile, λ_{max}, nm ($\varepsilon/10^{-4}$ M^{-1} cm^{-1})}: 229 (1.37),

265 (0.37), 400 (0.22); Anal. Calc. for $C_{24}H_{29}ClF_6N_4PRh$ (656.84): C, 43.89; H, 4.45; N, 8.53. Found: C, 44.02; H, 4.39; N, 8.61%.

*2.5.8. [Cp*Ir(L4)Cl]PF_6 (**8**)*

Yield: 65 mg (43%); IR (KBr, cm^{-1}): 3458(s), 3383(s), 2922(m), 1643(s), 1603(m), 1567(m), 1447(m), 844(s); ^{1}H NMR (400 MHz, DMSO-d_6): δ = 8.97 (d, 1H, *J* = 4.0 Hz, $CH_{(py)}$), 8.31-8.34 (m, 2H, $CH_{(py)}$), 7.85 (t, 1H, $CH_{(py)}$), 7.79 (d, 1H, *J* = 8.0 Hz, $CH_{(Ar)}$), 7.44 (t, 1H, $CH_{(Ar)}$), 7.19-7.23 (m, 2H, $CH_{(Ar)}$), 6.99-7.03 (m, 3H, NH_2, $CH_{(Ar)}$), 2.46 (s, 3H, CH_3), 1.59 (s, 15H, $CH_{(Cp^*)}$); HRMS-APCI (m/z): 601.17 $[M\text{-}PF_6]^+$; UV–Vis {Acetonitrile, λ_{max}, nm ($\varepsilon/10^{-4}$ M^{-1} cm^{-1})}: 256 (0.53), 361 (0.20); Anal. Calc. for $C_{24}H_{29}ClF_6N_4PIr$ (746.15): C, 38.63; H, 3.92; N, 7.51. Found: C, 38.74; H, 4.03; N, 7.63%.

3. Results and discussion

3.1. Synthesis of ligands and complexes

The azine Schiff-base ligands (L1-L4) were prepared by the reaction of 2-pyridylamidrazone and the respective aldehyde or ketone in absolute ethanol medium. The complexes (**1**-**8**) were synthesized by the reaction of Rh/Ir metal precursors with the azine Schiff-base ligands. The cationic complexes were isolated with PF_6 counter ion. All these metal complexes were obtained in good yields and are yellow in color. They are stable in air as well as in solid state, and are non-hygroscopic. These complexes are soluble in common organic solvents such as dichloromethane, acetonitrile and acetone but insoluble in diethyl ether and hexane. All the synthesized ligands and complexes were fully characterized by spectroscopic techniques.

3.2. Spectroscopic characterization of ligands

The infrared spectra of the free ligand shows characteristic stretching frequencies for NH_2, OH, C=N and C=C groups. The NH_2 and OH stretching frequencies for the azine ligand appeared in the range of 3300-3500 cm^{-1}. The C=C and C=N stretching frequencies were observed in the range of 1550-1626 cm^{-1}. The proton NMR spectra of the ligands displayed signals in the range of 7.30-8.57 ppm assignable to the protons of the pyridine ring. The imine protons for L1 and L2 are located at 8.60 and 8.59 ppm respectively. The methoxy proton signal was observed as a singlet for L1 at 3.80 ppm. The methyl protons of L3 and L4 were observed as a singlet at 2.62 and 2.39 ppm respectively. The hydroxyl proton resonance for the ligands appeared in the range of 11.5-11.9 ppm. The aromatic protons of the ligand appeared as doublet, triplet and multiplet in the range of 6.21-7.29 ppm. The $[M+H]^+$ molecular ion peak for the ligands are shown in the experimental section which are found to be in good agreement with the expected range. The electronic spectra of the free ligands are shown in (Figure S1). The electronic spectra of the free ligands show absorption bands in the range of 210-360 nm. The band in the range of 210-250 nm can be assigned as π-π^* and n-π * transition. The band around 300-370 nm is due to the intermolecular charge transfer transition within the whole molecule [41].

3.3. Spectroscopic characterization of complexes

The IR spectra of the complexes show sharp bands around 842-846 cm^{-1} due to the P-F stretching frequency of the counter ion [42]. The OH and NH_2 stretching vibrations in the complexes were found around 3300-3500 cm^{-1}. The retaining of the OH and NH_2 stretching frequencies indicates that they are not involved in bonding to the metal center. The strong absorption band for $\nu_{C=N}$ around 1630-1650 cm^{-1} at higher wave numbers as compared to the free

ligand around 1615-1626 cm^{-1} suggest that the coordination to the metal occurs through the imine and pyridine nitrogen.

The proton NMR spectra of the metal complexes show that the ligand resonance signals are shifted downfield as compared to that of the free ligand. These signals are shifted downfield because of the ligand coordination to the metal atom. The imine proton signal was observed in the range of 9.0-9.13 ppm for complexes (**1**-**4**). The hydroxyl proton resonance for the complexes appeared in the range of 10.1-12.5 ppm respectively. The appearance of the hydroxyl proton signal indicates that the hydroxyl group is not involved in bonding to the metal atom. The pyridine ring protons also showed downfield signals comprising of doublet and triplet in the range of 7.75-8.96 ppm. The NH_2 protons were observed as a singlet for complexes (**1**-**4**) in the range of 7.35-7.37 ppm respectively. The methoxy proton resonance for complexes (**1** and **2**) appeared as a singlet at 3.81 and 3.83 ppm. The aromatic proton signals for complexes appeared in the range of 6.50-7.86 ppm as doublet, triplet and multiplet. The methyl proton signal for complexes (**5**-**8**) appeared as a singlet around 2.46-2.48 ppm respectively. In addition to the signals for the ligand protons, a sharp singlet was observed for all the complexes between 1.58-1.63 ppm respectively corresponding to the methyl protons of the Cp* ring. In the mass spectra of the complexes (**1**–**6**) the peaks at m/z: 507.12, m/z: 597.18, m/z: 477.12, m/z: 567.17, m/z: 491.13 and m/z: 581.20 can be assigned as $[M\text{-}PF_6\text{-}HCl]^+$ ion peaks respectively. Whereas, the mass spectra of the complex **7** and **8** displayed molecular ion peaks at m/z: 511.12 and 601.17 which corresponds to the $[M\text{-}PF_6]^+$ ion.

The electronic spectra of the complexes were recorded in acetonitrile at 10^{-4} M concentration at room temperature and the plot is shown in (Figure S2). The electronic spectra of complexes display two absorption band in the higher energy region around 210-330 nm. The

316 bands in the higher energy UV region can be assigned as ligand centered or intra ligand π-π* and
317 n-π*transition. The Rh(III) and Ir(III) complexes provides filled dπ (t_{2g}) orbitals which can
318 interact with low lying π* orbitals (C=N) of the ligand. The band in the lower energy region
319 around 345-405 nm can be assigned as Rh (dπ) or Ir (dπ) to π* ligand metal to ligand charge
320 transfer (MLCT) transition [43].

321 *3.4. Molecular structures of complexes*

322 The molecular structures of some of the respective complexes have been elucidated by
323 single crystal X-ray analysis. Suitable single crystals were attached to a glass fibre and
324 transferred into the Oxford Diffraction Xcalibur Eos Gemini diffractometer. The crystallographic
325 details and structure refinement details are summarized in Table 1. The geometrical parameters
326 around the metal atom involving ring centroid are listed in Table S1. In all these complexes the
327 ligand is coordinated to the metal atom in a similar manner with N∩N binding mode. Complex
328 (**1**) and (**8**) crystallized in triclinic system with space group P$\bar{1}$. Complex (**8**) crystallized with
329 one PF_6 and one chloride counter ion. Complex (**3**) and (**4**) crystallized in monoclinic system
330 with space group $P2_1/c$ whereas complex (**7**) crystallized in monoclinic system with space group
331 $P2_1$.

332 All these complexes display a typical three-legged piano stool geometry around the metal
333 center with coordination sites occupied by one chloride group, two σ bonded nitrogen atoms
334 from chelating azine ligand and the pentamethylcyclopentadienyl (Cp*) ring in η^5 manner. The
335 metal atom in all these complexes is situated in a pseudo-octahedral arrangement with the azine
336 ligand coordinating through the pyridine and azine nitrogen atoms forming a five membered
337 metallocycle. In complexes (**1**), (**3**), (**4**) and (**7**) the M-N bond length {2.088(5), 2.099(3),
338 2.098(4) and 2.102(4) Å} from pyridine is comparatively shorter than the azine nitrogen-metal

distances {2.135(5), 2.116(3), 2.105(4) and 2.159(4) Å}, which are similar to those, reported with similar complexes [24, 44]. However in complex (**8**) the metal-nitrogen distance from pyridine {2.102(5) Å} is comparatively larger than azine nitrogen-metal distance, which is {2.096(5) Å}. The C=N bond length of the coordinated nitrogen in complex (**1**), (**3**), (**4**) and (**8**) is longer than that of the uncoordinated C=N (Table S1) which could be due to the back bonding of electron from metal (dπ) to π* orbital of the ligand. But in complex (**7**), a reverse pattern has been observed where the C=N bond length of the coordinated nitrogen {1.346(7) Å} is shorter than uncoordinated C=N {1.358(7) Å} bond. The average M-C distances are {2.159 (**1**), 2.1534 (**3**), 2.1616 (**4**), 2.1528 (**7**) and 2.1726 (**8**) Å} while the distance between the metal to Cp* centroid ring is in the range of 1.758–1.793 Å respectively. The M-Cl bond lengths {2.3976(15) (**1**), 2.4172(9) (**3**), 2.4190(12) (**4**), 2.4242(16) (**7**) and 2.4220(17) (**8**) shows no significant differences and is comparable to previously reported values (Table 1) [45-48]. The bite angle N(1)-Rh(1)-N(2) values are 75.10(19) (**1**), 75.09(11) (**3**), and 75.44(17) (**7**) whereas in complex (**4**) and (**8**) the bite angle values are N(1)-Ir(1)-N(2) values are 74.99(14) (**4**) and 75.26(18) respectively which probably indicates an inward bending of the coordinated pyridyl and azine group [49]. The bond angles N(1)-M-Cl(1) and N(2)-M-Cl(1) in complexes are comparable to the piano stool arrangement about the metal atom and is comparable to reported values for closely related systems [50-52]. Further the crystal packing in complex (**1**) is stabilized by weak intermolecular hydrogen bonding C-H·····O (2.702 Å) between the hydrogen atom from methoxy group and oxygen atom of the hydroxyl group and C-H·····Cl (2.793 Å) interaction between CH_3 group of Cp* and chloride atom (Figure S3). These interactions play a significant role in the formation of supramolecular motifs.

On the other hand in the crystal structure of complex (**3**) and (**4**) two types of intramolecular hydrogen bonding has been observed; the first one between the uncoordinated nitrogen atom of the azine linkage with the hydrogen atom of the hydroxyl group O-H·····N (1.916 and 1.908 Å) and the second between the hydrogen atom from NH_2 and uncoordinated azine nitrogen atom N-H·····N (2.323 and 2.328 Å) (Figure 4). The selected hydrogen bonding distances and angles for complex (**3**) and (**4**) are given in (Table 2). Also the crystal packing in complex (**3**) and (**4**) is further stabilized by two different C-H·····Cl interaction between the Cl atom attached to metal M (where M = Rh/Ir) with hydrogen atom of pyridine ring and NH_2 (Figure S4). Complex (**7**) shows C-H·····π (2.832 and 2.937 Å) interactions between the methyl hydrogen atom and Cp* moiety and between pyridine ring and hydrogen atom of Cp* group respectively (Figure S5). Interestingly the crystal packing in complex (**8**) leads to a dimeric unit via intermolecular C-H·····Cl interaction between the chloride counter ion and hydrogen atom from pyridine ring, NH_2 and Cp* group (Figure S6).

3.5. Chemosensitivity studies

The complexes (**1**-**8**) were tested for their cytotoxicity against cancer cell line HT-29 (human colorectal cancer), and non-cancer cell line ARPE-19 (human retinal epithelial cells). The response of the cell lines HT-29 to the test complexes and cisplatin (**1**-**8**) is presented in graphical form in Figure 5 and in tabular form in Table 3. All the complexes tested were found to be active against HT-29 cancer cell line (IC_{50}< 30 μM). Complex (**5**) was the most potent among all the complexes with (IC_{50} value of 96.93 ± 5.31 μM). However all the complexes were less potent than cisplatin (IC_{50} value of 0.25 ± 0.11 μM against HT-29). The selectivity index (SI) defined as the ratio of IC_{50} values in ARPE19 cells divided by the IC_{50} value of cancer cell line demonstrates that all the complexes are effective against cancer cell with SI values ranging from

1.01 to 2.11 (Table S2). Moreover although complex (**5**) showed more selectivity than other complexes for HT-29 cancer cell, however its selectivity was significantly lower than cisplatin where SI value is 25.64 (Figure 6).

3.6. Optimized geometry

The comparison of the geometric parameters (selected bond lengths and bond angles) of the optimized structures and the crystal structures of the complexes (**1**, **3**, **4**, **7** and **8**) are listed in Table S3. All the metal complexes are found to be closed shell structures. The calculated bond lengths and the bond angles of the complexes are in good agreement with the experimental data indicating the reliability of the theoretical method (B3LYP/6-31G**/LanL2DZ) used in the present study. It should be noted that for complexes (**3**, **4**, **7** and **8**), the M(1)-N(2) (where M = Rh/Ir) bond length is slightly longer than the M(1)-N(1) bond length whereas for complex (**1**), a reverse pattern has been observed (Table S3).

3.7. Charge distribution

The charges on the individual atoms for the metal complexes obtained from NBO analysis are listed in Table S4. The charges on the Rh atom in the complexes (**1**), (**3**), (**5**) and (**7**) are 0.136, 0.200, 0.216 and 0.214 e whereas the charges on Ir for complexes (**2**), (**4**), (**6**) and (**8**) are 0.186, 0.252, 0.268 and 0.214 e respectively. These NBO charges on Rh and Ir are comparatively lower than their formal charge of +3 which suggests that the ligand transfers their negative charge to the respective rhodium and iridium metal on complex formation. In metal complexes (**1**-**8**), the charge on Cl ranges between -0.439 e (Complex-**1**) to -0.394 e (Complex-**4**). In isolated ligands, the charge on N(1) ranges between -0.416 and –0.417 e whereas for N(2) it ranges between -0.324 e and -0.348 e. It should be noted that for isolated ligands as well as for complexes (**1**-**8**), the negative charges on N(1) (-0.385, -0.381, -0.372, -0.373, -0.369, -0.398, -

0.368 and -0.373 e) are slightly higher than the charges on N(2) (-0.258, -0.253, -0.284, -0.283, -0.305, -0.297, -0.311 and -0.305 e). On complex formation, the negative charge on the N(1) and N(2) reduces slightly giving an indication of the charge transfer on Rh and Ir in metal complexes. The population of the 4d ($4d_{xy}$, $4d_{xz}$, $4d_{yz}$, $4d_{x^2-y^2}$ and $4d_{z^2}$) orbital of Rh complexes and 5d orbital of Ir complexes are shown in Table S5. The orbital occupations of each orbital (nd_{xy}, nd_{xz}, nd_{yz}, $nd_{x^2-y^2}$ and nd_{z^2}) for all the complexes are comparatively higher in rhodium complexes than iridium complexes. In free Rh(III) and Ir(III) state, the population of nd_{xy}, nd_{xz} and nd_{yz} are 2.0, 2.0 and 2.0 e and the other two orbitals remain vacant. But on complex formation, the population on nd_{xy}, nd_{xz} and nd_{yz} orbital gets reduced whereas the nd_{x2-y2} and nd_{z^2} orbitals gain some population as indicated in Table S5. For most of the complexes, the population of 4d and 5d orbital containing the same ligand follow similar pattern of filling, except for the complexes containing ligand L1 where the nd_{xz} orbital population is slightly lower and $nd_{x^2-y^2}$ is higher as compared to the other complexes.

3.8. Frontier molecular orbitals and absorption spectra

The molecular orbital representation of the complexes along with their HOMO, LUMO energies and HOMO-LUMO energy gaps are shown in Figure 7. The HOMO-LUMO energy gap can be used as an important parameter in analyzing the chemical reactivity and kinetic stability of a molecule. This energy gap is also related to the hardness/softness of a chemical species [53]. The lower HOMO-LUMO energy gap is a suitable condition where a molecule can be excited easily and thereby increasing its reactivity and decreasing its kinetic stability whereas higher energy gap can lead to more kinetic stability but less reactivity. The HOMO-LUMO energy gaps for all the complexes (**1**-**8**) are found to be 3.20, 2.98, 3.63, 3.46, 3.61, 3.60, 3.68 and 3.59 eV respectively. The gap is slightly lower for the iridium complexes as compared to rhodium

complexes containing the same ligand indicating the reactivity of Ir complexes over the complexes containing Rh metal. The % contribution of molecular orbital analysis as shown in Table S6, predicts that the most percentage of HOMO is located on the ligand itself except for complex (**2**) and (**8**) where as it is mostly present on the Ir metal. On the other hand, LUMO is located on the ligand for complexes (**1**) (about 97%), (**2**) (91%), (**4**) (89%), (**6**) (92%) and (**8**) (69%) whereas for complexes (**3**) (40%), (**5**) (35%) and (**7**) (38%), it is located on the Rh metal.

The electronic absorption spectra were calculated using the TD-DFT method in acetonitrile solvent employing PCM model. The calculated and the experimental absorption data, HOMO-LUMO energy gaps, and the character of electronic transitions are listed in Table 4. The H→L transitions for complexes (**1**), (**4**) and (**6**) occurring at 417, 444 and 441 nm corresponds to ILCT character, for complexes (**2**) and (**8**) at 463 and 440 nm corresponds to MLCT character whereas for complexes (**3**), (**5**) and (**7**) at 532, 519 and 518 nm corresponds to LMCT character. These MLCT character can be assigned for $d\pi(M)\rightarrow\pi^*(L)$ transitions whereas the ILCT character are for $\pi\rightarrow\pi^*$ transitions. It should be noted that all LMCT transitions are occurring at higher wavelength regions (i.e. > 500 nm). In good agreement with the experimental data, the TD-DFT calculations shows few MLCT transitions at 358 nm complex (**2**), 332 nm, complex (**4**), 334 nm complex (**6**) and 372, 358 nm complex (**8**). However, in the range between 340-400 nm, few LMCT, ILCT and LLCT transitions have also been observed (Table 4).

4. Conclusion

In summary, we have synthesized four new azine Schiff-base ligands and its rhodium and iridium half-sandwich complexes. All these complexes and ligands were full characterized by various spectroscopic techniques. The ligands under study preferably bind to the metal in a bidentate N∩N fashion using pyridine and one azine nitrogen atom. Our attempt to synthesize

dinuclear rhodium and iridium complexes with NN′ and NO bonding was however unsuccessful irrespective of molar ratio of metal to ligand where as in the presence of base, it leads to decomposition of the reaction. These complexes possess some important intramolecular and intermolecular hydrogen bonding and also possess some weak non-covalent interactions, particularly C-H·····Cl and C-H·····π interactions. Chemosensitivity activity of the complexes against HT-29 cancer cell demonstrates that the complexes are active however complex (**5**) was found to be the most potent among all other complexes. Theoretical studies reveal that the HOMO-LUMO energy gap is lower for iridium complexes indicating better reactivity over the rhodium complexes. TD-DFT calculations were carried out in order to evaluate the electronic transitions occurring in the metal complexes, which are in good agreement with the experimental results. The charge distribution analysis (using NBO analysis) of these complexes helps to understand how the charges on nitrogen atom (which are coordinating to the metal) are delocalized on complex formation. Especially, the NBO charges, on rhodium and iridium confirm that the ligands transfer their negative charge to the respective metal on complex formation. The lower HOMO-LUMO energy gap leads to greater chemical reactivity but lesser kinetic stability and vice versa. Furthermore, the nature of HOMO and LUMO illustrate the electronic origin of the lowest energy transition and the resulting electronic reorganization. Moreover, the molecular orbital analysis was helpful to understand and locate the % contribution of HOMO and LUMO on different fragments of the complexes, which is otherwise not possible to predict from experimental data.

Acknowledgements

Sanjay Adhikari and Dipankar Sutradhar thanks UGC, New Delhi, India for providing financial assistance in the form of university fellowship (UGC-Non-Net). We thank DST-PURSE

SCXRD, NEHU-SAIF, Shillong, India for providing Single crystal X-ray analysis and other spectral studies. AKC thanks Computer centre, NEHU, for computational facilities.

Supplementary material

CCDC **1477976** (**1**), **1477977** (**3**), **1477978** (**4**), **1477979** (**7**) and **1477980** (**8**) contains the supplementary crystallographic data for this paper. These data can be obtained free of charge via www.ccdc.cam.ac.uk/data_request/cif, by e-mailing data_request@ccdc.cam.ac.uk, or by contacting The Cambridge Crystallographic Data Centre, 12, Union Road, Cambridge CB2 1EZ, UK; Fax: +44 1223 336033.

References

[1] G. Gasser, I. Ott, N. Metzler-Nolte, J. Med. Chem. 54 (2011) 3.

[2] L. Ronconi, P.J. Sadler, Coord. Chem. Rev. 251 (2007) 1633.

[3] Y.K. Yan, M. Melchart, A. Habtemariam, P.J. Sadler, Chem. Commun. (2005) 4764.

[4] B. Therrien, Coord. Chem. Rev. 253 (2009) 493.

[5] U. Sliwinska, F.P. Pruchnik, S. Ulaszewski, M. Latocha, D. Nawrocka-Musial, Polyhedron 29 (2010) 1653.

[6] M.A. Scharwitz, I. Ott, Y. Geldmacher, R. Gust, W.S. Sheldrick, J. Organomet. Chem. 693 (2008) 2299.

[7] M.A. Nazif, J.-Amade Bangert, I. Ott, R. Gust, R. Stoll, W.S. Sheldrick, J. Biol. Inorg. Chem. 103 (2009) 1405.

[8] M. Gras. B. Therrien, G. Suss-Fink, A. Casini, F. Edafe, P.J. Dyson, J. Organomet. Chem. 695 (2010) 1119.

[9] Y. Geldmacher, M. Oleszak, W.S. Sheldrick, Inorg. Chim. Acta 393 (2012) 84.

[10] R. Bieda, I. Ott, M. Dobroschke, A. Prokop, R. Gust, W.S. Sheldrick, J. Biol. Inorg. Chem. 103 (2009) 698.

[11] Z. Liu, P.J. Sadler, Acc. Chem. Res. 47 (2014) 1174.

[12] G. Gupta, A. Garci, B.S. Murray, P.J. Dyson, G. Fabre, P. Trouillas, F. Giannini, J. Furrer, G. Suss-Fink, B. Therrien, Dalton Trans. 42 (2013) 15457.

[13] S. Mukhopadhyay, R.K. Gupta, R.P. Paitandi, N.K. Rana, G. Sharma, B. Koch, L.K. Rana, M.S. Hundal, D.S. Pandey, Organometallics 34 (2015) 4491.

[14] J. De Pasquale, I. Nieto, L.E. Reuther, C.J. H-Gervasoni, J.J. Paul, V. Mochalin. M. Zeller, C.M. Thomas, A.W. Addison, E.T. Papish, Inorg. Chem. 52 (2013) 9175.

[15] Y. Geldmacher, K. Splith, I. Kitanovic, H. Alborzinia, S. Can, R. Rubbiani, M.A. Nazif, P. Wefelmeier, A. Prokop, I. Ott, S. Wolfl, I. Neundorf, W.S. Sheldrick, J. Biol. Inorg. Chem. 17 (2012) 631.

[16] Z. Liu, I. Romero-Canelon, A. Habtemariam, G.J. Clarkson, P.J. Sadler, Organometallics 33 (2014) 5324.

[17] Z. Liu, A. Habtemariam, A.M. Pizarro, S.A. Fletcher, A. Kisova, O. Vrana, L. Salassa, P.C.A. Bruijnincx, G.J. Clarkson, V. Brabec, P.J. Sadler, J. Med. Chem. 54 (2011) 3011.

[18] J. Safari, S. Gandomi-Ravandi, RSC Adv. 4 (2014) 46224.

[19] Z. Xu, L.K. Thompson, D.O. Miller, Inorg. Chem. 36 (1997) 3985.

[20] M. Ghedini, A.M.M. Lanfredi, F. Neve, A. Tiripicchio, J. Chem. Soc. Chem. Commun. (1987) 847.

[21] E.-Q. Gao, S.-Q. Bai, Y.-F. Yue, Z.-M. Wang, C.-H. Yan, Inorg. Chem. 42 (2003) 3642.

[22] Y.-F. Yue, C.-J. Fang, E.-Q. Gao, C. He, S.-Q. Bai, S. Xu, C.-H. Yan, J. Mol. Struct. 875

(2008) 80.

[23] Z. Xu, L.K. Thompson, D.A. Black, C. Ralph, D.O. Miller, M.A. Leech, J.A.K. Howard, J. Chem. Soc., Dalton Trans. (2001) 2042.

[24] K.T. Prasad, G. Gupta, A.V. Rao, B. Das, K.M. Rao, Polyhedron 28 (2009) 2649.

[25] G. Gupta, S. Gloria, S.L. Nongbri, B. Therrien, K.M. Rao, J. Organomet. Chem. 696 (2011) 2014.

[26] D.D. Perrin, W.L.F. Armarego, Purification of Laboratory Chemicals, fourth ed., Butterworths Heinemann, London, 1996.

[27] C. White, A. Yates, P.M. Maitlis, D.M. Heinekey, Inorg. Synth. 29 (2007) 228.

[28] G.M. Sheldrick, Acta Crystallogr. Sect. A 64 (2008) 112.

[29] G.M. Sheldrick Acta Crystallogr. Sect. C 71 (2015) 3.

[30] L.J. Farrugia, J. Appl. Crystallogr. 32 (1999) 837.

[31] R.M. Phillips, P.B. Hulbert, M.C. Bibby, N.R. Sleigh, J.A. Double, Br. J. Cancer. 65 (1992) 359.

[32] R.A. Kaner, S.J. Allison, A.D. Faulkner, R.M. Phillips, D.I. Roper, S.L. Shepherd, D.H. Simpson, N.R. Waterfield, P. Scott, Chem. Sci. 7 (2016) 951.

[33] M.J. Frisch et al., GAUSSIAN 09, Revision C.01, Gaussian Inc, Walling-ford, CT, 2009.

[34] A.D. Becke, J. Chem. Phys. 98 (7) (1993) 5648.

[35] C. Lee, W. Yang, R.G. Parr, Phys. Rev. B 37 (2) (1988) 785.

[36] E. Cances, B. Mennucci, J. Tomasi, J. Chem. Phys. 107 (1997) 3032.

[37] A.E. Reed, L.A. Curtiss, F. Weinhold, Chem. Rev. 88 (1988) 899.

[38] M.E. Casida, in: J.M. Seminario (Ed.), Recent Developments and Applications in Modern Density Functional Theory, Theoretical and Computational Chemistry, vol. 4, Elsevier, Amsterdam, 1996.

[39] L. Skripnikov, Chemissian v4.36, A computer program to analyse and visualise quantum-chemical calculations, 2015.

[40] F. Weldon, L. Hammarstrom, E. Mukhtar, R. Hage, E. Gunneweg, J.G. Haasnoot, J. Reedijk, W.R. Browne, A.L. Guckian, J.G. Vos, Inorg. Chem. 43 (2004) 4471.

[41] C.U. Dueke-Eze, T.M. Fasina, M.J. Mphahlele, Asian J. Chem. 25 (2013) 8505.

[42] S.D. Dwivedi, A.K. Singh, S.K. Singh, S. Sharma, M. Chandra, D.S. Pandey, Eur. J. Inorg. Chem. (2008) 5666.

[43] P. Govindaswamy, Y.A. Mozharivskyj, K.M. Rao, Polyhedron 24 (2005) 1710.

[44] D.L. Davies, J. Fawcett, R. Krafczyk, D.R. Russell, J. Organomet. Chem. 581 (1997) 545.

[45] P. Chellan, K.M. Land, A. Shokar, A. Au, S.H. An, D. Taylor, P.J. Smith, T. Riedel, P.J. Dyson, K. Chibale, G.S. Smith, Dalton Trans. 43, (2014) 513.

[46] G. Gupta, G. Sharma, B. Koch, S. Park, S.S. Lee, J. Kim, New.J.Chem. 37 (2013) 2573.

[47] K.S. Singh, Y.A. Mozharivskyj, C. Thone, M.R. Kollipara, J. Organomet. Chem. 690 (2005) 3720.

[48] N.R. Palepu, S.L. Nongbri, J.R. Premkumar, A.K. Verma, K. Bhattacharjee, S.R. Joshi, S. Forbes, Y.A. Mozharivskyj, R. Thounaojam, K. Aguan, M. R. Kollipara, J. Biol. Inorg. Chem. 20 (2015) 619.

[49] S.K. Singh, M. Chandra, D.S. Pandey, M.C. Puerta, P. Valerga, J. Organomet. Chem. 689 (2004), 3612.

[50] R. Payne, P. Govender, B. Therrien, C.M. Clavel, P.J. Dyson, G.S. Smith, J. Organomet. Chem. 729 (2013) 20.

[51] A.P. Walsh, W.W. Brennessel, W.D. Jones, Inorg. Chim. Acta 407 (2013) 131.

568 [52] M. Kalidasan, S.H. Forbes, Y. Mozharivskyj, M.R. Kollipara, Inorg. Chim. Acta 421
569 (2014) 218.
570 [52] Y. Hanifehpour, B. Mirtamizdoust, S.W. Joo, J Inorg Organomet Polym. 22 (2012) 916.

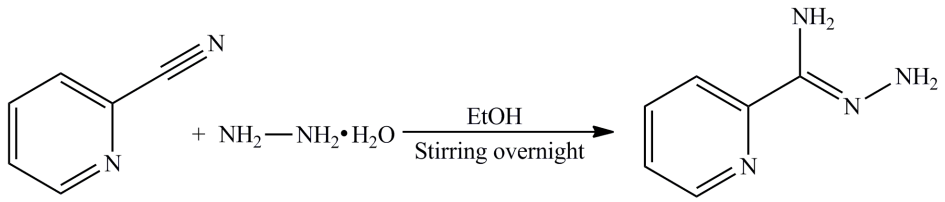

571

572 Scheme-1 Synthesis of 2-pyridylamidrazone

573

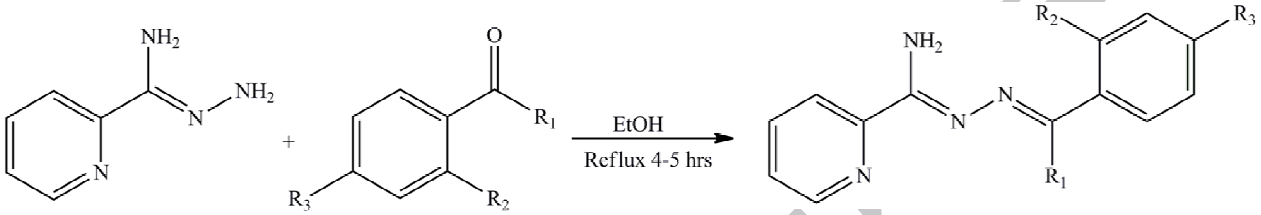

L1: R_1 = H, R_2 = OH, R_3 = OCH_3
L2: R_1 = R_3 = H, R_2 = OH
L3: R_1 = CH_3, R_2 = OH, R_3 = H
L4: R_1 = CH_3, R_2 = R_3 = H

574

575 Scheme-2 Preparation of ligands (L1-L4)

576

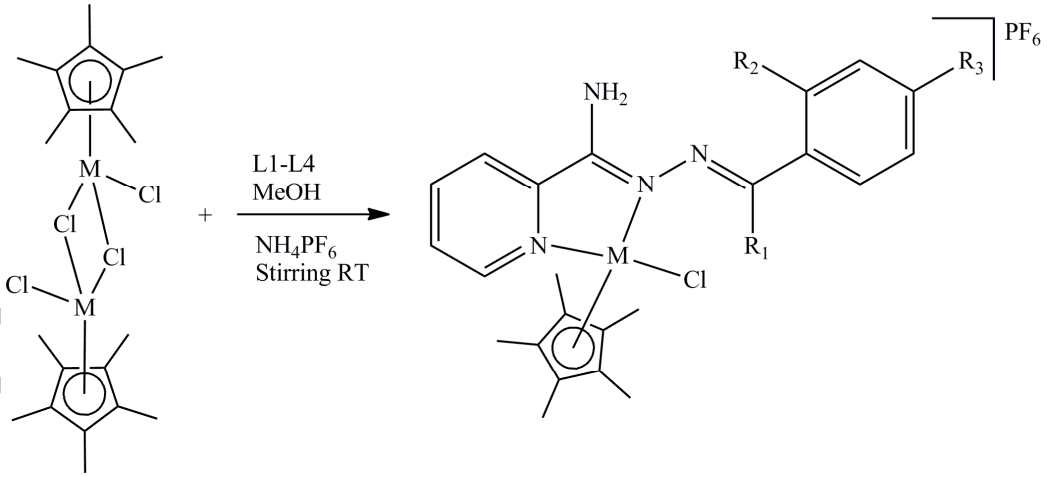

M = Rh (**1**) (**3**) (**5**) (**7**)
Ir (**2**) (**4**) (**6**) (**8**)

577

578 Scheme-3 Preparation of metal complexes (**1**-**8**)

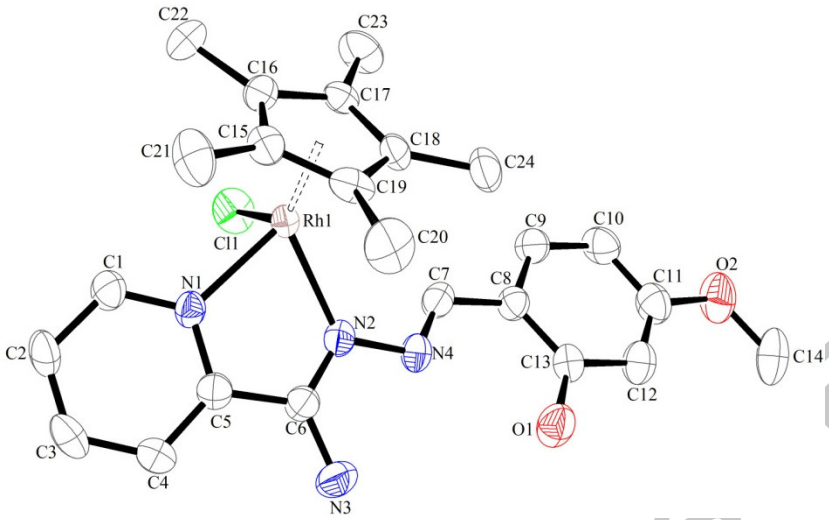

Figure 1 ORTEP diagram of complex [Cp*RhCl(L1)Cl]PF_6 (**1**) with 50% probability thermal ellipsoids. Hydrogen atoms and counter ions are omitted for clarity.

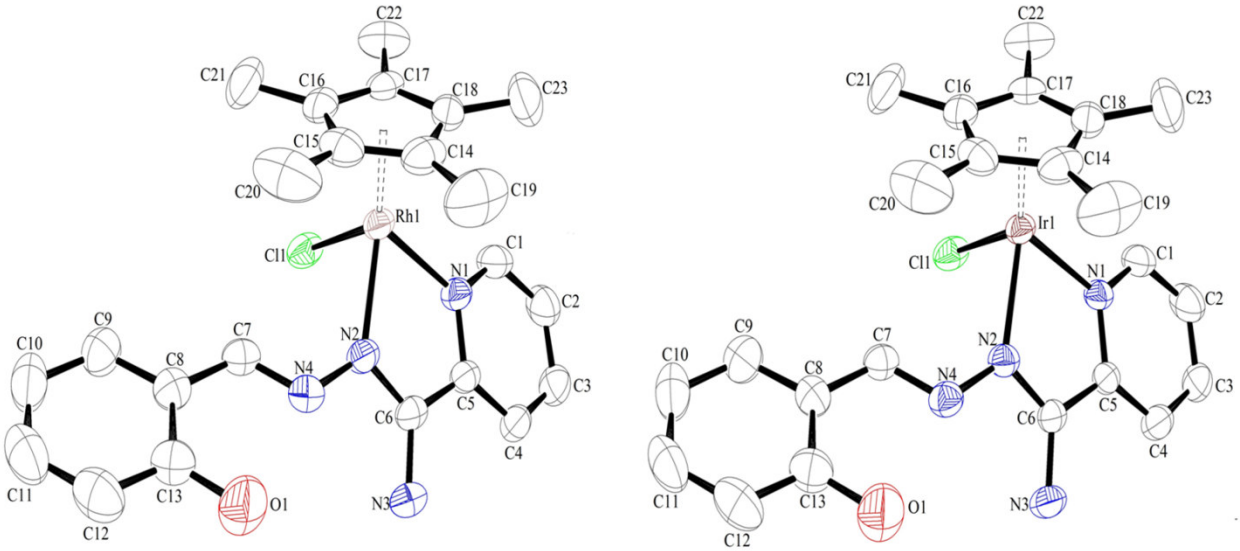

Figure 2 (a) ORTEP diagram of complex [Cp*RhCl(L2)Cl]PF_6 (**3**) and (b) ORTEP diagram of complex [Cp*IrCl(L2)Cl]PF_6 (**4**) with 50% probability thermal ellipsoids. Hydrogen atoms and counter ions are omitted for clarity.

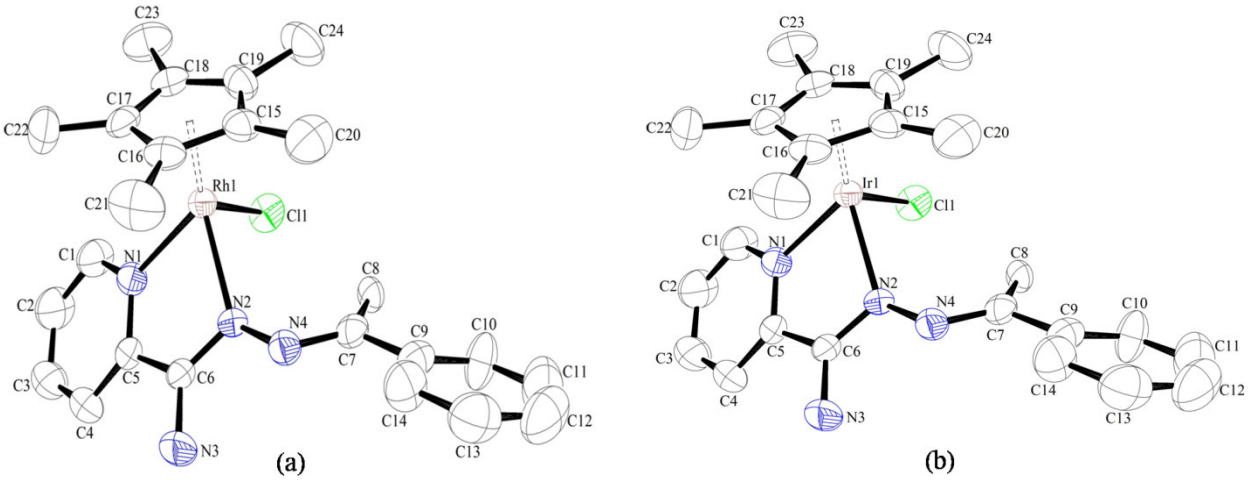

Figure 3 (a) ORTEP diagram of complex [Cp*Rh(L4)Cl]PF_6 (**7**) and (b) ORTEP diagram, of complex [Cp*IrCl(L4)Cl]PF_6 (**8**) with 50% probability thermal ellipsoids. Hydrogen atoms and counter ions are omitted for clarity.

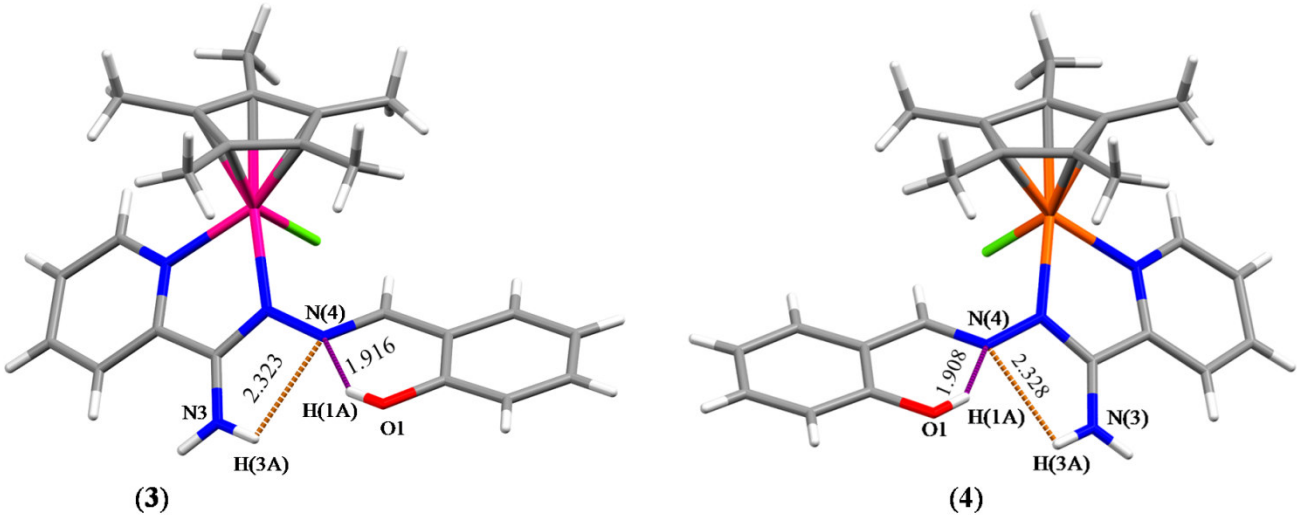

Figure 4 Crystal structure of complexes (**3**) and (**4**) showing intramolecular hydrogen bonding.

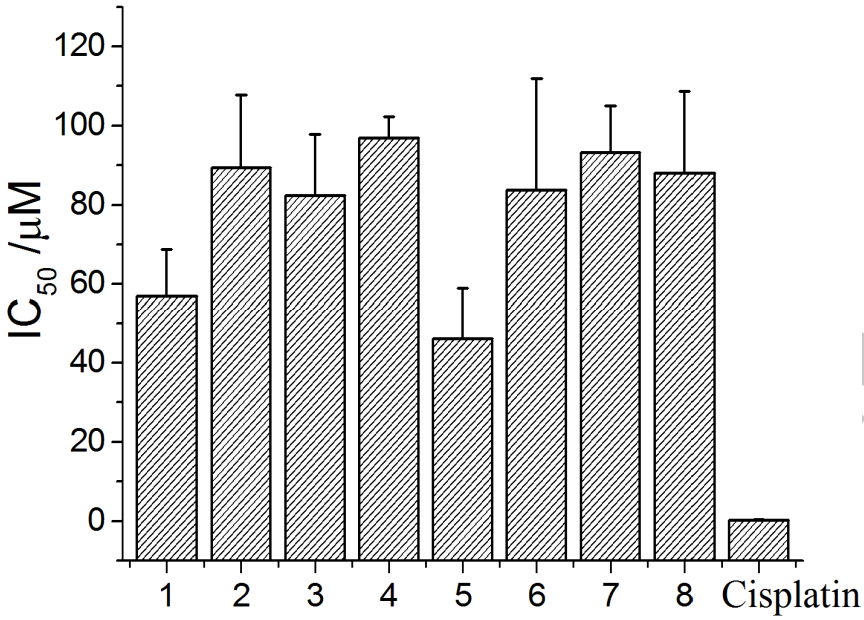

Figure 5 Response of HT-29 (human colorectal cancer) to compounds (**1**-**8**) and cisplatin. Cell were exposed to compounds (**1**-**8**) for 96 hours. Each value represents the mean ± standard deviation from three independent experiments.

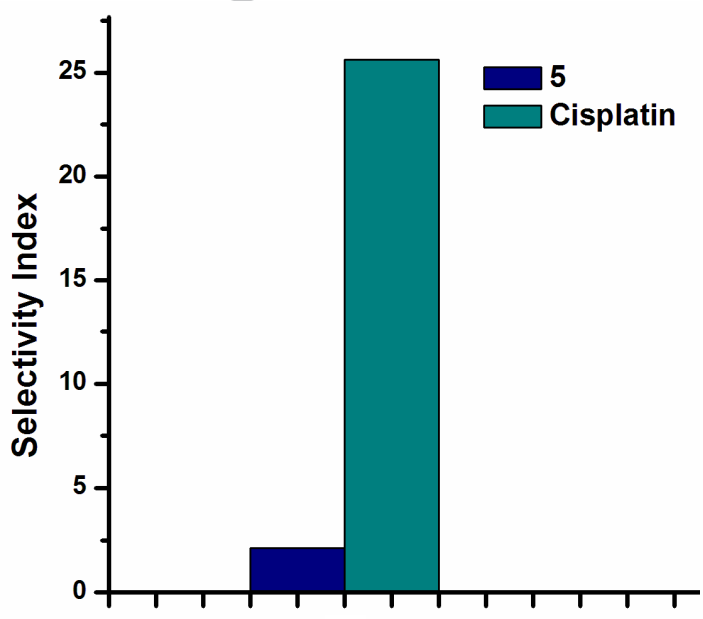

Figure 6 Graph showing selectivity index of complex **5** and cisplatin against HT-29 cancer cell line. The selectivity index is defined as the IC_{50} of ARPE19 cell divided by the IC_{50} of tumour cell line.

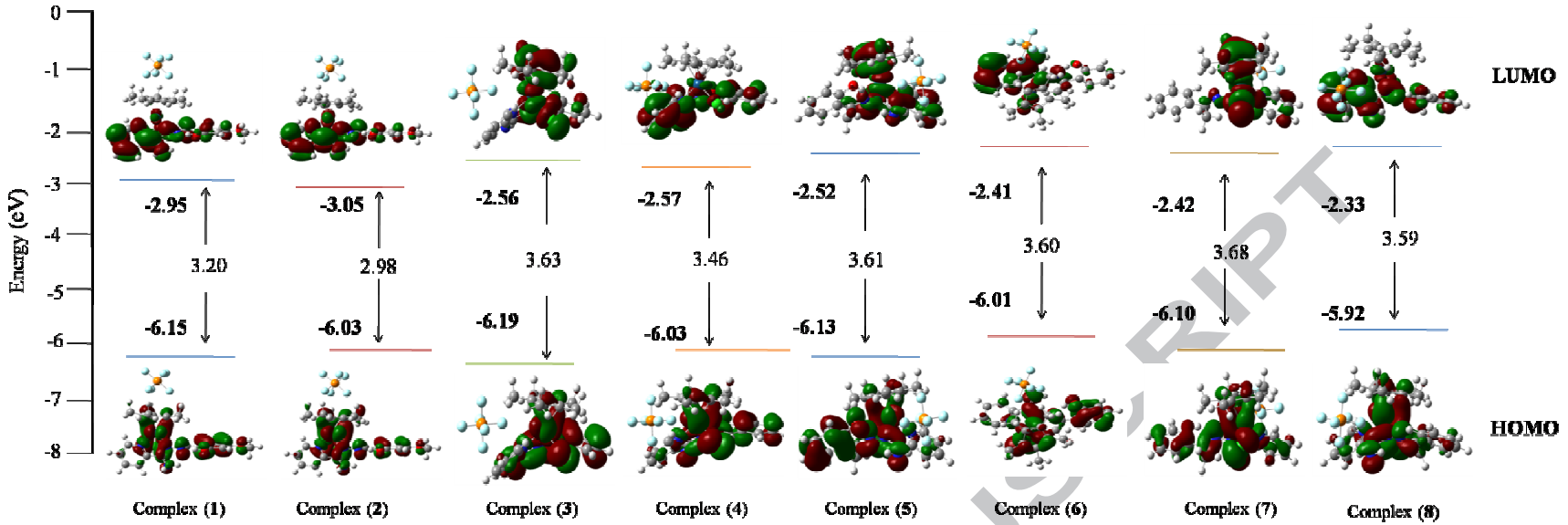

Figure 7 HOMO, LUMO energies and their energy gap of complexes (**1–8)**

606 Table 1. Crystal structure data and refinement parameters of complexes.

Complexes	[**1**] PF_6	[**3**] PF_6	[**4**] PF_6	[**7**] PF_6	[**8**] PF_6 Cl
Empirical formula	$C_{24}H_{29}ClN_4O_2F_6PRh$	$C_{23}H_{27}ClF_6N_4OPRh$	$C_{23}H_{27}ClF_6N_4OPIr$	$C_{24}H_{29}ClF_6N_4PRh$	$C_{24}H_{29}Cl_2F_6N_4PIr$
Formula weight	688.84	658.82	748.11	656.84	781.58
Temperature (K)	298(2)	293(2)	293(2)	293(2)	293(2)
Wavelength (Å)	0.71073	0.71073	0.71073	0.71073	0.71073
Crystal system	triclinic	monoclinic	monoclinic	monoclinic	triclinic
Space group	*P T*	*P2₁/c*	*P2₁/c*	*P2₁/c*	*P T*
a (Å)/α (°)	8.3893(7)/89.370(6)	10.6710(6)/90	10.7019(5)/90	38.850(5)/90	7.9976(4)/87.496
b (Å)/β (°)	10.5533(7)/86.439(6)	17.0730(8)/92.708(4).	17.0860(9)/93.062(4)	7.9488(5)/98.027(4)	12.4774(4)/82.086(4)
c (Å)/γ (°)	16.6554(11)/71.182(7)	14.5390(8)/90	14.6118(9)/90	28.562(4)/90	14.6442(6)/72.596(4)
Volume ($Å^3$)	1393.00(18)	2645.8(2)	2668.0(2)	1344.83(10)	1381.15(10)
Z	2	4	4	2	2
Density (calc) (Mg/m^{-3})	1.642	1.654	1.862	1.622	1.879
Absorption coefficient (μ) (mm^{-1})	0.836	0.874	5.231	0.857	5.148
F(000)	696	1328	1456	664	762
Crystal size (mm^3)	0.23 x 0.21 x 0.21	0.21 x 0.19 x 0.04	0.23 x 0.23 x 0.21	0.22 x 0.20 x 0.120	0.19 x 0.12 x 0.09
Theta range for data collection	3.174 to 28.654°.	3.33 to 26.73°.	3.31 to 26.37°.	3.386 to 28.842°.	3.23 to 26.37°.
Index ranges	-11<=h<=10, -12<=k<=13, -22<=l<=20	-13<=h<=10, -10<=k<=21, -12<=l<=18	-13<=h<=7, -21<=k<=19, -16<=l<=18	-9<=h<=9, -12<=k<=22, -14<=l<8	-8<=h<=9, -15<=k<=15, -17<=l<18
Reflections collected	10811	9506	10081	5614	7889
Independent reflections	6286 [R(int) =0.0717]	5375 [R(int) = 0.0268]	5422 [R(int) = 0.0277]	4000 [R(int) = 0.0268]	5335 [R(int) = 0.0296]
Completeness to theta = 25.00°	99.57 %	99.5 %	99.2 %	99.2 %	94.8 %
Absorption correction	Semi-empirical from equivalents	Semi-empirical from equivalents	Semi-empirical from equivalents	Semi-empirical from equivalents	Semi-empirical from equivalents
Refinement method	Full-matrix least-squares on F^2	Full-matrix least-squares on F^2	Full-matrix least-squares on F^2	Full-matrix least-squares on F^2	Full-matrix least-squares on F^2
Data/restraints/parameters	6286/0/362	2375/0/330	5422/0/340	4000/1/340	5335/0/349
Goodness-of-fit on F^2	1.197	1.063	1.026	1.041	1.046
Final R indices [I>2sigma(I)]	R1 = 0.0703, wR2 = 0.1706	R1 = 0.0440, wR2 = 0.0895	R1 = 0.0340, wR2 = 0.0630	R1 = 0.0394, wR2 = 0.0822	R1 = 0.0368, wR2 = 0.0875
R indices (all data)	R1 = 0.0855, wR2 = 0.1772	R1 = 0.0592, wR2 = 0.0968	R1 = 0.0500, wR2 = 0.0683	R1 = 0.0462, wR2 = 0.0858	R1 = 0.0431, wR2 = 0.0912
Largest diff. peak and hole ($e.Å^{-3}$)	0.583 and -0.461	0.520 and -0.543	1.102and -1.143	0.512 and -0.478	1.828 and -1.071
CCDC No.	1477976	1477977	1477978	1477979	1477980

607 Structures were refined on F_0^2: $wR_2 = [\Sigma[w(F_0^2 - F_c^2)^2] / \Sigma w(F_0^2)^2]^{1/2}$, where $w^{-1} = [\Sigma(F_0^2)+(aP)^2+bP]$ and $P = [\max(F_0^2, 0)+2F_c^2]/3$.

608 Table-2. Selected hydrogen bonding distances (Å) and angles (°) of complexes **3** and **4**.

Complexes	D-H·····A	H····A (Å)	D·····A (Å)	D·····H (Å)	∠D─H···A(°)
3	O(1)-H(1A)·····N(4)	1.916	2.638	0.820	146.39
	N(3)-H(3A)·····N(4)	2.323	2.624	0.860	100.76
4	O(1)-H(1A)·····N(4)	1.908	2.634	0.820	146.90
	N(3)-H(3A)·····N(4)	2.328	2.629	0.860	100.78

609

610 Table-3 Response of HT-29 (human colorectal cancer) to complexes (**1**-**8**) and cisplatin. Each

611 value represents the mean ± standard deviation from three independent experiments.

Complexes	IC_{50} (μM)	
	HT-29	ARPE-19
1	56.95 ± 11.76	85.31 ± 14.86
2	89.42 ± 18.33	93.45 ± 11.34
3	82.32 ± 15.55	83.03 ± 14.76
4	96.93 ± 5.31	>100
5	46.17 ± 12.78	97.39 ± 4.53
6	83.74 ± 28.17	>100
7	93.16 ± 11.84	>100
8	88.09 ± 20.63	>100
Cisplatin	0.25 ± 0.11	6.41 ± 0.95

612

613 Table 4. The energy gap, theoretical and experimental absorption bands, electronic transitions

614 and dominant excitation character for various singlet states of the complexes (**1**-**8**) calculated

615 with TD-DFT method.

The most important orbital excitations	Calculated λ (nm)	Energy gap E (eV)	Oscillator strength (f)	Dominant excitation Character	Experimental λ (nm)
			Complex (**1**)		
H→L	417.16	3.20	0.2051	L1→L1(ILCT)	
H-2→L	359.64	3.53	0.0542	Cl→L1(LLCT)	352.21
H→L+2	355.41	4.03	0.0120	L1→L1(ILCT)	
H-4→L+2	338.40	4.89	0.0139	L1→L1(ILCT)	
H-1→L+4	278.91	4.73	0.0248	L1→L1(ILCT)	276.0
H-6→L	282.81	4.54	0.0073	L1→L1(ILCT)	
H-6→L+2	275.41	5.37	0.0050	L1→L1(ILCT)	
H-11→L	235.62	5.08	0.0216	Rh→L1(MLCT)	233.3
H-5→L+4	233.62	5.74	0.0480	Cl→L1(LLCT)	

H-6→L+3	232.46	5.46	0.0105	L1→L1(ILCT)	
			Complex (**2**)		
H→L	462.76	2.98	0.0644	Ir→L1(MLCT)	
H→L+3	358.38	4.64	0.0191	Ir→Cp*(MLCT)	347.0
H-4→L	340.55	4.01	0.0075	L1→L1(ILCT)	
H-5→L+1	273.73	5.11	0.0470	Cp*→L1(LLCT)	266.0
H-2→L+4	266.79	5.33	0.1540	L1→Ir(LMCT)	
			Complex (**3**)		
H→L	532.04	3.63	0.0087	L2→Rh(LMCT)	
H-2→L+1	348.95	4.11	0.0369	L2→L2(ILCT)	344.10
H→L+2	345.72	3.84	0.0128	L2→Rh(LMCT)	
H-1→L+2	344.68	4.10	0.0089	Cl+L2→Rh(LMCT)	
H-3→L	336.07	4.24	0.0047	Cl→Rh(LMCT)	
H→L+4	289.42	4.85	0.0063	L2→L2(ILCT)	286.1
H-6→L	285.32	5.14	0.0163	Cl+L2→Rh(LMCT)	
H-5→L+1	282.59	4.98	0.0391	L2→L2(ILCT)	
H-4→L+4	237.16	5.74	0.0422	L2→L2(ILCT)	234.30
H-5→L+3	234.58	5.74	0.0161	L2→L2(ILCT)	
			Complex (**4**)		
H→L	444.09	3.46	0.0355	L2→L2(ILCT)	
H-2→L	362.56	3.91	0.0077	L2→L2(ILCT)	346.1
H-1→L+1	332.29	3.80	0.0076	Rh+L2→L2(MLCT/ILCT)	
H→L+3	329.46	4.48	0.0468	L2→L2(ILCT)	
H-4→L	324.35	4.53	0.0265	Cl+Cp*→L2(LLCT)	
H-4→L+2	294.35	5.47	0.0164	Cl+Cp*→L2(LLCT)	292.21
H-1→L+2	288.71	4.74	0.0048	Rh+L2→Rh+L2	
H-8→L+3	212.19	6.47	0.0387	L2→L2(ILCT)	210.9
H-6→L+4	210.71	6.56	0.0399	Cl→L2(LLCT)	
H-2→L+5	210.22	6.26	0.0669	L2→L2(ILCT)	
			Complex (**5**)		
H→L	519.01	3.61	0.0076	L3→Rh(LMCT)	
H-2→L+2	338.46	4.30	0.0120	Cl→L3(LLCT)	332.0
H-4→L+1	326.16	4.56	0.0052	L3→Rh(LMCT)	
H-1→L+4	271.36	5.01	0.265	L3→L3(ILCT)	268.0
H-2→L+4	267.30	5.21	0.0177	Cl→L3(LLCT)	
H-5→L+4	232.84	5.83	0.0498	L3→L3(LLCT)	229.0
H-10→L+2	229.44	6.14	0.0127	Rh+L3→L3(MLCT/ILCT)	
			Complex (**6**)		
H→L	441.76	3.60	0.0160	L3→L3(ILCT)	
H-2→L+1	334.33	4.45	0.0109	Ir→L3(MLCT)	330.0
H-1→L+1	328.24	4.33	0.1160	L3→L3(ILCT)	
H-7→L	268.58	5.42	0.0159	Ir→L3(MLCT)	256.0
H-6→L	264.64	5.25	0.0304	Cl→L3(LLCT)	
H-1→L+4	260.56	5.17	0.0350	L3→L3(ILCT)	
			Complex (**7**)		
H→L	518.07	3.68	0.0071	L4→Rh(LMCT)	
H-1→L	448.90	4.05	0.0132	Cl→Rh(LMCT)	400.0
H-1→L+1	397.25	4.09	0.0148	Cl→Rh(LMCT)	
H-1→L+4	269.94	5.23	0.0297	Cl→L4(LLCT)	265.0
H-2→L+3	262.52	5.20	0.0465	Cl→L4(LLCT)	

H→L+5	231.04	5.66	0.0547	L4→L4(ILCT)	229.0
			Complex (**8**)		
H→L	439.65	3.59	0.0196	Ir→L4(MLCT)	
H-1→L+2	371.55	4.79	0.0381	Ir→L4(MLCT)	361.0
H-1→L	358.22	4.0	0.0349	Ir→L4(MLCT)	
H-2→L+3	257.57	5.29	0.0359	Cl→Cp*(LLCT)	256.0
H-4→L+3	255.65	5.61	0.0142	L4→Cp*(LLCT)	

616